Computers and Chemical Engineering 179 (2023) 108458

Contents lists available at ScienceDirect

Computers and Chemical Engineering

journal homepage: www.elsevier.com/locate/cace

Computational fluid dynamics modeling of aerosol particle transport through lung airway mucosa☆,☆☆

Blake A. Bartlett [a,b], Yu Feng [a], Catherine A. Fromen [c], Ashlee N. Ford Versypt [a,d,e,f,*]

[a] School of Chemical Engineering, Oklahoma State University, Stillwater, OK 74078, USA
[b] School of Chemical, Biological and Materials Engineering, University of Oklahoma, Norman, OK 73019, USA
[c] Department of Chemical & Biomolecular Engineering, University of Delaware, Newark, DE 19716, USA
[d] Department of Chemical and Biological Engineering, University at Buffalo, The State University of New York, Buffalo, NY 14260, USA
[e] Department of Biomedical Engineering, University at Buffalo, The State University of New York, Buffalo, NY 14260, USA
[f] Institute for Artificial Intelligence and Data Science, University at Buffalo, The State University of New York, Buffalo, NY 14260, USA

ARTICLE INFO

Dataset link: CFDparticleLungMucosa (Original data)

Keywords:
Lung-aerosol dynamics
Diffusion
Nanoparticles
Inhaled particles
Mucociliary clearance

ABSTRACT

Delivery of aerosols to the lung can treat various lung diseases. However, the conducting airways are coated by a protective mucus layer with complex properties that make this form of delivery difficult. Mucus is a non-Newtonian fluid and is cleared from the lungs over time by ciliated cells. Further, its gel-like structure hinders the diffusion of particles through it. Any aerosolized treatment of lung diseases must penetrate the mucosal barrier. Using computational fluid dynamics, a model of the airway mucus and periciliary layer was constructed to simulate the transport of impacted aerosol particles. The model predicts the dosage fraction of particles of a certain size that penetrate the mucus and reach the underlying tissue, as well as the distance downstream of the dosage site where tissue concentration is maximized. Reactions that may occur in the mucus are also considered, with simulated data for the interaction of a model virus and an antibody.

1. Introduction

Lung diseases afflict hundreds of millions of people and are some of the most common causes of death worldwide (World Health Organization, 2020). Existing methods of treating these diseases are limited by poor targeting to the lungs when medications are given orally or intravenously and require rigorous, long-term, often invasive medication to achieve remission in pathogenic diseases (Feng et al., 2018; Kolewe et al., 2021). Other diseases are chronic but suffer similar limitations in treatment methods, inhaled or otherwise. The idea of treating lung diseases at the source is an attractive one, offering a noninvasive route to locally dose a diseased area that also minimizes side effects; however, several problems still exist (Henning et al., 2010; Ruge et al., 2013; Hastedt et al., 2016; Duncan et al., 2018). A significant physical challenge to overcome is the mucociliary clearance mechanism (Fig. 1), which utilizes rhythmically waving ciliated cells to constantly push the mucus layer that coats the lungs upward towards the throat (Ruge et al., 2013). This system serves as a natural defense against infection and particle buildup but simultaneously acts as a barrier to drug delivery (Duncan et al., 2016; Carlson et al., 2018; Chen et al., 2019).

The anatomical interface between the airways and the lung epithelium is comprised of a fluid bilayer, with the highly viscous mucus layer on top of the more watery periciliary layer (PCL) (Fahy and Dickey, 2010; Taherali et al., 2018) (Fig. 1). The PCL allows the cilia to beat without catching in the mucus and acts as a lubricant that allows the mucus to slide along the interface (Cone, 2005; Chateau et al., 2018). The mucus is primarily water, but a network of glycoproteins known as mucins causes it to move as a bulk "sheet" when propelled by the cilia. Mucins are rich in cysteine, making them largely anionic (Cone, 2005). Disulfide bonds are a large contributor to the structure of the network. However, large portions of the chains are neutral, making mucins also appreciably lipophilic (Murgia et al., 2018). The PCL also contains mucins, but these are tethered to cilia and do not form the tangled net that is seen in the mucus layer. This makes the PCL a "brush" that prevents mixing of the two layers and maintains the viscous character of the PCL compared to the more elastic character of the mucus layer (Button et al., 2012). Because the cilia are regular in size, the PCL is consistently ≈ 7 μm thick through the entire conducting airways (Fahy and Dickey, 2010). In contrast, the mucus layer thickness varies significantly depending on location. Goblet cells, which secrete

☆ Research carried out at the School of Chemical Engineering, Oklahoma State University, Stillwater, OK 74078 USA.
☆☆ A preliminary version of this work, doi: 10.1101/2021.10.18.464809v2, was deposited in bioRxiv.
* Correspondence to: 507 Furnas Hall, University at Buffalo, The State University of New York, Buffalo, NY 14260, USA.
E-mail address: ashleefv@buffalo.edu (A.N. Ford Versypt).

https://doi.org/10.1016/j.compchemeng.2023.108458
Received 6 May 2023; Received in revised form 30 August 2023; Accepted 13 October 2023
Available online 16 October 2023

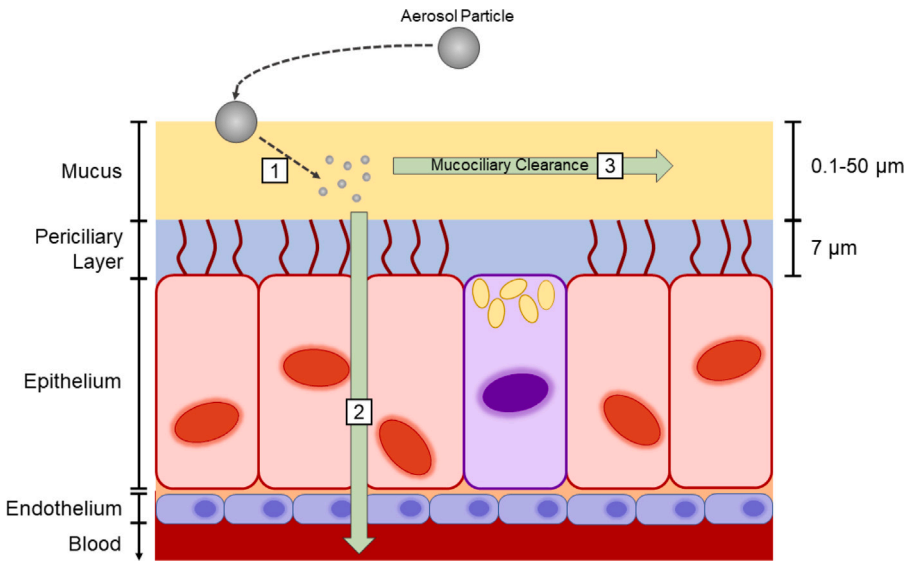

Fig. 1. Methods of particle clearance from the lung mucosa. (1) Particles can be lodged in the mucus, where they may be degraded or consumed by macrophages before subsequent mucociliary clearance. (2) Particles can diffuse across the mucosa and be taken up into the tissue or even the bloodstream. (3) Most commonly, particles are either unable to diffuse adequately or are immobilized by some means and cleared by mucociliary clearance.

mucus, are present throughout the respiratory tract and are more plentiful in the first lung generations, *i.e.,* the trachea and bronchi (Clarke and Pavia, 1980). Thus, the mucus layer increases in thickness from the terminal bronchioles to the trachea. Mucus can be as thin as 0.1 μm at the respiratory bronchioles (extending to generation 19) and as thick as 100 μm at the trachea (Chateau et al., 2018; Taherali et al., 2018; Nawroth et al., 2019). At the deepest levels of the respiratory tract, the alveolar region has no mucus layer at all. The velocity at which mucus is cleared depends on a variety of factors that vary significantly between individuals including age, health, and history of smoking.

The tangled network of mucins in the mucus layer gives the layer marked elastic properties so that it behaves as a viscoelastic gel, which for our purposes is approximated as a shear-thinning non-Newtonian fluid (Lai et al., 2007; Cone, 2008; Norton et al., 2011; Murgia et al., 2018). This shear-thinning relationship exists in healthy individuals (and is the reason coughing is an effective method of clearing mucus (King et al., 1985; Taherali et al., 2018)) but is accentuated in obstructive lung diseases like cystic fibrosis, chronic obstructive pulmonary disease (COPD), and asthma. In these diseases, mucin production is elevated, causing the mucus to become much thicker and more difficult to clear than in the healthy case (Duncan et al., 2016). This "thickening" of the mucus, along with other factors like dehydration or dysfunction in electrolyte concentrations, can lead to a collapse of the PCL as one or both layers become too viscous for the cilia to beat effectively (Taherali et al., 2018). Using a non-Newtonian mathematical model for the mucus allows for a single simulation that can be applied to both healthy and diseased states at the discretion of the user without extensive viscosity data, which is particularly lacking for diseased states.

The rheological properties of lung mucus must be taken into account to successfully treat lung disease via an inhaled aerosol, and the drug particles must have certain properties to pass through the mucus quickly and efficiently. A model of these fluid layers can predict the effective penetration of a delivered pharmaceutical or can be modified to simulate the infectivity of a pathogen. While researchers have been optimistic about the possibility of aerosol treatments for various lung conditions and diseases for decades (Yeates et al., 1975; Wolff, 1986; Lethem, 1993), poor characterization of the mucosa has been a limitation to progress. Experimental and theoretical developments in the understanding of the production of nanoparticles, aerosolization, and delivery to specific sites in the lung have made these treatments much more attainable (Tang et al., 2009; Kleinstreur and Feng, 2013; Feng et al., 2019), but the literature lacks a generalized model for predicting behavior in the mucus. Models that exist largely focus on cilial beating (Smith et al., 2008; Norton et al., 2011) or individual pores of the mucus layer (Cu and Saltzman, 2009; Hansing and Netz, 2018a,b). Other models are simplified to the point of ignoring fluid movement or the existence of multiple fluid layers (Kirch et al., 2012; Sims et al., 2019)–both of which leave questions about locating dosage sites or macroscopic behavior unanswered. The purpose of this research is to help fill that gap by producing a model that simulates the lung airway mucosal layers (Fig. 2) for a region of the conducting airways and that predicts the behavior of applied aerosolized particles. In this paper, we construct a computational fluid dynamics model of the lung airway mucosa informed by properties taken from the literature. After defining the model in Section 2, we show model predictions of the dosage distribution of particles of different sizes that penetrate mucus of various thicknesses to reach the underlying tissue, and we show the distance downstream of the dosage site where epithelial concentration is maximized for various cases. We also consider reactions to account for interactions between a model virus and an antibody delivered to the mucus.

2. Methods

2.1. Model geometry, mesh, and boundary conditions

We used COMSOL Multiphysics 5.6 for modeling convection and diffusion through the mucus and PCL. The model geometry represents a cross-section of the mucosa at any particular location in the conducting airways. We assumed that the conducting airways are radially symmetric; thus, we consider a 2D rectilinear domain (Fig. 2). The domain does not need to be expanded to the left of the dosage site as fluid convective velocity is several orders of magnitude higher than diffusive velocity; therefore, backflow is negligible. The thickness of the simulated domain is dependent on the lung location being simulated but is always on the scale of microns, so all geometrical dimensions for the model are on this scale. The thickness of the periciliary (lower) layer is effectively constant throughout the conducting airways at 7 μm. The length of the conducting airways is on the scale of decimeters (Chateau et al., 2018). While the width of the model domain is set small enough to assume no significant changes in mucus thickness over the simulation domain,

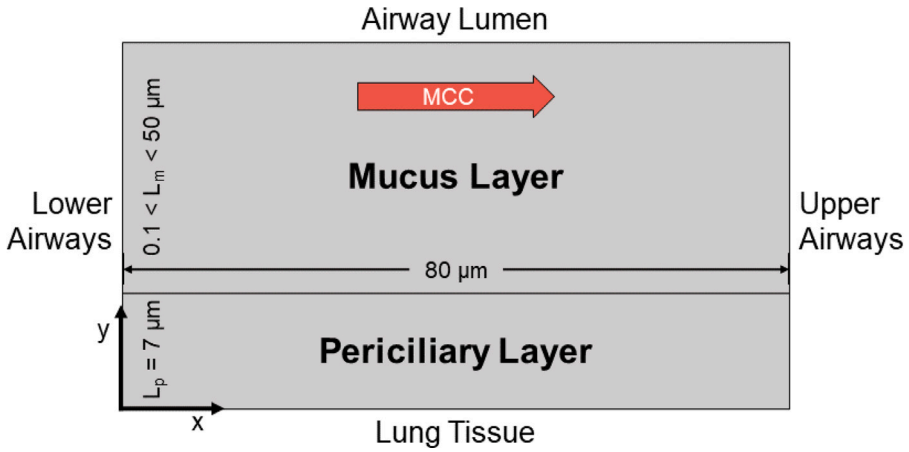

Fig. 2. Example of the geometry used in the model. The top layer is the mucus and is open to the conducting airways, also called the lumen. The bottom layer is the periciliary layer; the cilia beat through this layer and are attached to cells of the lung epithelium. Mucus flows from the respiratory bronchioles to the larynx (Nawroth et al., 2019), and this directionality of the mucociliary clearance (MCC) is simulated as left to right in the diagram. L_m is the thickness of the mucus layer, which varies by region, and L_p is the thickness of the periciliary layer, which is uniform.

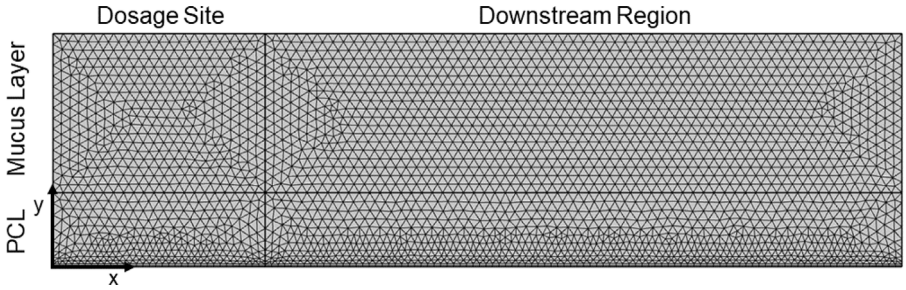

Fig. 3. Mesh for the simulation domain. Four rectangles compose the simulation domain. In clockwise order from the top left, these represent the dosage region of the mucus layer (where the dosage is applied on the top surface at the air-mucus interface), the downstream region of the mucus layer, the downstream region of the periciliary layer (PCL), and the dosage region of the periciliary layer.

the specific domain width value is partially arbitrary. All simulation domains shown in this paper have a total width of 80 μm, as this value is sufficiently large to observe epithelial concentration maxima for all studied particle sizes.

The simulation domain of the model is two-dimensional, consisting of a series of four rectangles, arranged such that both a dosage site and a "downstream" area can be simulated with two distinct fluid layers (Fig. 3). Where the edges of these rectangles meet, COMSOL forms a union between them, such that there is no formal boundary condition separating them and all meshing is continuous. The top two rectangles represent the mucus layer, and the bottom two rectangles represent the underlying PCL. The rectangles on the left have the same fluid properties as the rectangles on the right with respect to their layer, but the left side functions as the dosage site, whereas the right side represents the fluid upstream of this site. For these simulations, we assume that concentration at the top edge of the dosage site is uniform to simulate behavior averaged across inhalation patterns, radial distribution, and other random transient effects related to the delivery of the aerosol itself, although an *in vivo* case likely follows an orientation-dependent distribution curve (Feng et al., 2018; Kolewe et al., 2021).

We use COMSOL Multiphysics to generate a mesh for the model using the "fine" resolution setting following a mesh independence test. This triangular mesh provides discrete points at which each relevant system of equations is solved, resulting in a two-dimensional field of behavior across the simulation domain. The mesh may be refined manually at the price of increased computation times.

The upper boundary of the mucus is open to the airways, where airflow from normal breathing imparts a negligible amount of shear on the surface of the highly viscoelastic fluid (Cone, 2008). We consider this air–liquid interface as being governed by a slip condition. Conversely, the lower boundary of the PCL borders the static epithelium and is subject to a no slip condition. Bulk fluid moves from the left boundary of both layers to an outlet at the right boundaries without accumulation within the simulation domain. The mucus and PCL average velocities are specified (Table 1) and held constant. High viscosity and low velocity mean that the mucus has a small Reynolds number, moving in the fully developed laminar flow regime. Using fluid layer depth as the characteristic length, the Reynolds numbers for the two layers are approximately $Re_{muc} = 1.2 \times 10^{-6}$ for a mucus depth of 15 μm and $Re_{pcl} = 4.0 \times 10^{-4}$ for a periciliary layer depth of 7 μm. Even though $Re \ll 1$, flow was not modeled as creeping flow (also called Stokes flow) because the linearized simplified form of the Navier–Stokes equation used for Stokes flow is not able to properly account for non-Newtonian fluid dynamics in its normal formulation. Drug particles (molecules, aerosolized liquid droplets, or dry nanoparticles) are treated as continuous dilute species for modeling purposes. For the simulations shown here, the dilute species enters from the airways at a constant concentration constraint applied to the air-mucus interface (top surface of the top left rectangle in Fig. 3), which makes steady-state simulations possible. The dilute species may exit at the rightmost boundary—simulating mucociliary clearance —or at the bottom boundary—simulating uptake into the epithelium, which is assumed to occur instantaneously when the solute reaches the bottom boundary. This behavior is accomplished using outflow boundary conditions on these edges. The dilute species cannot cross the upper boundary, as this would imply that the applied particles may freely vaporize. Nothing prevents the dilute species from crossing the leftmost boundary as it is given an outflow boundary condition. In practice backflow does not

occur due to the differences in magnitude between convection and diffusion. At the initial condition, no drug is in the mucus or PCL.

With the dilute species inlet being a constant concentration constraint and instantaneous outflow boundary conditions (no accumulation of the dilute species within the domain), the model domain reaches a steady state after a "startup time" has elapsed. For a domain of this size, this time is about 1 s. This makes a time-independent study possible. The stationary solution is a major simplification of the physiological case, but such simulations are useful as they take a comparatively short time to compute and show long-term trends, most notably the concentration profiles. Targeted deposition technologies allow for drug to be concentrated in a single lobe of the lung (Islam and Feng, 2023), but the dosage is otherwise dispersed across a large surface area. A user may tune the model to fit the type of dispersal that is expected, such as using a time-dependent parabolic distribution function for the inlet rather than a constant concentration; this route potentially increases rigor at the cost of increased computational times and residual errors. Even with our simplified technique proposed here, future users can extend the work to consider tapering dosages along sequential segments of an expanded dosage region. For more intricate models of inhaled particle dispersal and transport in the airways, see the work of Feng and colleagues (Kleinstreur and Feng, 2013; Feng et al., 2018, 2019; Kolewe et al., 2021; Islam and Feng, 2023).

2.2. Model equations and parameters

In this study, mucus and PCL flows are considered laminar and incompressible. Nanoparticles are modeled as a continuous dilute species. The nanoparticle-laden mucosal flows are simulated by solving the following governing equations, including the conservation laws of mass and momentum. The convection–diffusion equation (*i.e.,* material balance equation) for the concentrations of particles and the possible products generated by reactions occurring within the mucosa is

$$\frac{\partial c_i}{\partial t} + \nabla \cdot (-D_i \nabla c_i) + u \cdot \nabla c_i = R_i \tag{1}$$

where c_i is the concentration of species i, D_i is diffusivity of species i, and u is fluid velocity. The first term represents accumulation in the domain, the second for diffusive transport, the third for convective transport, and the right side of the equation for the production or consumption of species as a result of chemical reactions. These equations require a value of diffusivity to be specified, which is defined later in this manuscript in (3). In the case where a chemical reaction is occurring to produce or consume the relevant species, the term R_i is defined as the net production rate of species i. If no reaction occurs, then $R_i = 0$. Other assumptions include constant density for the two layers (Norton et al., 2011), constant velocities for the clearance of the mucus layer and PCL (Matsui et al., 1998; Shete et al., 2014; Taherali et al., 2018), and equivalent diffusivity through the different layers. The fiber volume fraction for a healthy individual is in the range of 0.0005 to 0.01 (Hansing and Netz, 2018b). For all simulations in this manuscript, the fiber volume fraction was set to 0.0025. Mucin dimensions are within ranges reported by Lai et al. (2009). Table 1 includes the values or ranges of the parameters used for the simulations.

For the diffusivity of spherical particles in bulk solution, we use the Stokes–Einstein equation

$$D_0 = \frac{k_b T}{6\pi\mu r_s} \tag{2}$$

where k_b is the Boltzmann constant, T is absolute temperature, μ is the dynamic viscosity of the pure solvent (in this case water), and r_s is the Stokes radius of the solute particle. We allow r_s to vary throughout our simulations. However, mucins provide a steric hindrance to diffusion, so an appropriate effective diffusivity correlation (3) is used as a correction factor for the Stokes–Einstein result. The mucus is porous with an average pore size of around 150 nm (Button et al., 2012; Kim et al., 2016), but the network is not rigid. Mucus is reasonably described as a hydrogel, where diffusivity is a function of fiber size rather than a function of pore size. We solve for an effective diffusivity, D, for a solute moving through the mucus and PCL using a correlation from the literature that accounts for both steric and hydrodynamic interactions in a fibrous hydrogel in the first and second terms, respectively (Philips, 2000):

$$\frac{D}{D_0} = \exp\left(-0.84 f^{1.09}\right) \exp\left(-a\phi^b\right) \tag{3}$$

where ϕ is the fiber volume fraction, f is an adjusted volume fraction defined by

$$f = \left(1 + \frac{1}{\lambda}\right)^2 \phi, \tag{4}$$

$\lambda = r_f / r_s$, r_f is the fiber radius, r_s is the solute particle radius, and a and b are fitting factors for the hydrodynamic effects term defined as

$$a = 3.727 - 2.460\lambda + 0.822\lambda^2 \tag{5}$$

and

$$b = 0.358 + 0.366\lambda - 0.0939\lambda^2 \tag{6}$$

Eqs. (3)–(6) in their fully expanded forms are characterized by only three parameters: fiber radius (r_f), particle radius (r_s), and fiber volume fraction (ϕ). Particle radius is one of the primary design variables for this study, although fiber volume fraction may also vary with disease states (Cone, 2008; Button et al., 2012).

No specific pore size or shape is assumed in (3). Rather, hindrance is related to the likelihood that a diffusing particle will collide with a fiber. Additionally, (3) does not rely on Brinkman or effective medium approximations. The Brinkman equation is a variation of Darcy's law that is designed to describe flow in media where the grains of the media are themselves porous, and the equation requires measurement of effective viscosity. Effective medium theory as applied to these situations, in short, considers the mucus to be characterized only by its Darcy permeability (Johnson et al., 1996). Both effective viscosity and Darcy permeability are generally more difficult to calculate, measure, or estimate than r_s, r_f, and ϕ. Thus, (3) is more approachable than similar equations that rely on these approximations, and (3) also tends to fit data more accurately (Philips, 2000).

The form of the conservation of momentum equation used by the COMSOL Multiphysics software is

$$\rho \nabla \cdot (u) = 0 \tag{7a}$$

$$\rho (u \cdot \nabla) u = \nabla \cdot (-pI + \tau) \tag{7b}$$

$$\tau = \mu \left(\nabla u + (\nabla u)^{\mathrm{T}}\right) \tag{7c}$$

where ρ is the fluid density, p is fluid pressure, u is the fluid velocity, μ is the fluid viscosity, and I and τ denote the identity tensor and the stress tensor, respectively. Reported measurements of clearance rates were collected *in vivo* and thus already include the effects of gravity and breathing. Consequently, the gravity term is neglected from the momentum equation to avoid double counting of effects that were not decoupled in the experiments. Since the flow regime is open to the airways, the mucus moves by open channel flow, and flow is not pressure-driven. These equations constitute the Navier–Stokes equations for an incompressible fluid and are subject to boundary conditions as specified above.

Considering the relation of mucus viscosity to shear rate (Vélez-Cordero and Lauga, 2013), we model the mucus layer as a Carreau fluid (Shahsavari and McKinley, 2015). The Carreau model is used in other applications to simulate similar biological fluids with non-Newtonian characteristics like blood. The governing equation is

$$\mu_{eff}(\dot{\gamma}) = \mu_{inf} + (\mu_0 - \mu_{inf}) \left(1 + (\sigma\dot{\gamma})^2\right)^{\frac{n-1}{2}} \tag{8}$$

Table 1
Model parameters. PCL: periciliary layer.

Parameter	Definition	Value	Units	Ref.
ρ	Density of fluid	1000	kg/m^3	Norton et al. (2011)
T	Body temperature	310.15	K	–
μ	Viscosity of water at T	6.922×10^{-4}	Pa s	Korson et al. (1969)
u_{muc}	Mucus average velocity	5	mm/min in x-direction	Shete et al. (2014), Taherali et al. (2018)
u_{pcl}	PCL average velocity	2.4	mm/min in x-direction	Matsui et al. (1998)
C_{Ai}	Dosage concentration	1000	mol/m^3	–
L_m	Thickness of mucus	0.5 – 100	μm	Chateau et al. (2018), Taherali et al. (2018)
L_p	Thickness of PCL	7	μm	Fahy and Dickey (2010)
ϕ	Fiber volume fraction	0.0025	unitless	Hansing and Netz (2018b)
r_f	Mucin fiber radius	5	nm	Lai et al. (2009)
μ_0	Mucus zero-shear-rate viscosity	302	Pa s	Fitted to data (Lai et al., 2007)
σ	Mucus shear thinning parameter	8440	s	Fitted to data (Lai et al., 2007)
n	Mucus Carreau model exponent	0.375	s	Fitted to data (Lai et al., 2007)

where μ_{eff} is used as μ for the mucus layer in (7c), $\dot{\gamma}$ is the shear rate, $\mu_{inf} = 0$ is the infinite shear-rate viscosity (assuming that viscosity is small at infinite shear so that this term drops out of the equation), μ_0 is the zero-shear-rate viscosity, σ is the inverse of a characteristic shear rate at which shear thinning becomes important, and n is a power law exponent. Published experimental data was used to parameterize (8) for mucus. We used WebPlotDigitizer (Rohatgi, 2022) to digitize the data from Fig. 4 of in Lai et al. (2007). Then we used nonlinear least-squares regression to fit parameters μ_0, σ, and n to the Lai et al. (2007) data for cervicovaginal mucus. The values are listed in Table 1. It remains very difficult to obtain samples of human pulmonary mucus from healthy subjects. Sputum is often contaminated with saliva. Even samples collected from intubated patients are small in volume and contain an unknown ratio of mucus and periciliary fluid. The collection of such samples may exert mechanical stresses that induce secretion of water and further alter the rheological properties of the sample (Lai et al., 2009; Schuster et al., 2013). Further, collected samples are fragile and dramatically change when subjected to long-term storage, freezing, and many sample preparation techniques (Meziu et al., 2021), necessitating that samples must be analyzed when fresh. However, fresh, undiluted samples of healthy cervicovaginal mucus may be obtained fairly readily (Lai et al., 2007). Consequently, there is far more reliable rheological data for this type of human mucus. The raw data used here is from cervicovaginal mucus. Cone (2008) showed that all sources of mucus have very similar shear-thinning viscous behavior except ovulatory cervicovaginal mucus. As the data in Lai et al. (2007) is non-ovulatory, it was assumed to be a reasonable proxy for the viscous behavior of lung mucus.

2.3. Code availability

We have provided the COMSOL code and exported files for the results in a repository at https://github.com/ashleefv/CFDparticleLungMucosa (Bartlett and Ford Versypt, 2023).

3. Results and discussion

Before the diffusion of a dilute species was considered, we verified that the fluid velocity profile was realistic. In the biological system, the mucus layer is so viscous (due to the tangled network of mucins) that it moves largely as a single sheet. The PCL is more Newtonian due to conformational differences in mucin structure and is cleared more slowly because it does not respond elastically to cilial beating (Norton et al., 2011; Matsui et al., 1998; Hussong et al., 2013). Due to these differences in behavior, the Carreau correlation described in (8) was only applied to the mucus layer, and the PCL layer was treated as Newtonian with the viscosity of the PCL approximated as that for water. Average velocity u_{muc} in the x-direction was specified as 5 mm/min, an average *in vivo* tracheal mucus clearance rate (Shete et al., 2014; Taherali et al., 2018). Average velocity u_{pcl} was specified as 2.4 mm/min (Matsui et al., 1998). Fig. 4 shows the bulk movement of the mucus layer and the rapid drop in velocity in the PCL due to both the no-slip condition with the epithelium and property differences between the two layers. The average velocity of the mucus and PCL layers are defined independently using values from the literature (Matsui et al., 1998; Shete et al., 2014; Taherali et al., 2018), and COMSOL struggles to build a perfectly continuous fully-developed flow inlet from this input. As a result, the initial velocity profile in Fig. 4 includes some minor artifacts at the inlet (this can be seen more clearly near the inlet of Fig. 5). The profile stabilizes within a few microns of the inlet and does not affect the resultant diffusion profile.

Concurrent with the velocity profile arising from the viscous nature of the two fluids, it follows that the PCL is subject to a high shear rate (Fig. 5), as cilia beat through it constantly. Conversely, the mucus layer is subject to a low shear rate due to its elasticity (Fig. 5). In short, the shear rate is another measure of the mucus moving as a sheet, as the bulk mucus moves in response to cilial beating. The PCL is also responsive to this beating, but to a much smaller extent due to both the no-slip condition for the velocity profile and the much lower viscosity of the PCL. Another way of interpreting Fig. 5 is as a measure of resistance to movement. The high shear rate in the PCL is indicative of its Newtonian character, wherein the velocity profile exhibited by a fluid between a moving slab and an immobile plane is shear-driven (Matsui et al., 1998). The cause of this profile *in vivo* is cilial beating, but defining the velocity profile results in identical bulk fluid mechanics so cilia do not need to be explicitly modeled. Similar to the velocity profile, the values are nearly constant in the mucus but subject to a gradient in the PCL, albeit with high values in the PCL instead of the mucus in contrast to relative values of the corresponding layers in the velocity profile.

Once a velocity field was constructed, a drug dilute species was applied to study its transport through the domain. All simulations in this paper used a uniform delivery concentration of 1000 mol/m^3 = 1 mol/L along the lumen-side boundary of the dosage site. In the delivery of an actual drug, delivery would likely not be constant. Here, all mucus within the domain had a residence time of about 1 s due to mucociliary clearance, so this was considered a short enough timescale for constant delivery to be valid. Even the PCL, with an average velocity of 2.4 mm/min, sweeps the entire domain in 2 s. Thus for the simplified case of a constant uniform delivery along the dosage site, the system reaches steady state within a 2-second time scale. It was assumed that this concentration is sufficiently dilute that the delivered drug does not significantly change the volume of the system. COMSOL supports parameter sweeps, where a single solution of the system evaluates a range of parameters. This functionality was first utilized to compare the effect of mucus layer thickness (L_m) on drug penetration. Concentration profiles for three different mucus thicknesses, L_m = 5, 15, and 33 μm, were obtained (Fig. 6) to represent delivery to the bronchioles, bronchus, and trachea, respectively. Drug particle radius was held constant at $r_s = 20$ nm.

Parameter sweeps for drug particle radius were also performed (Fig. 7). Mucus thickness was held constant at L_m = 15 μm. Concentration profiles for particles of radii r_s = 5, 20, and 60 nm are

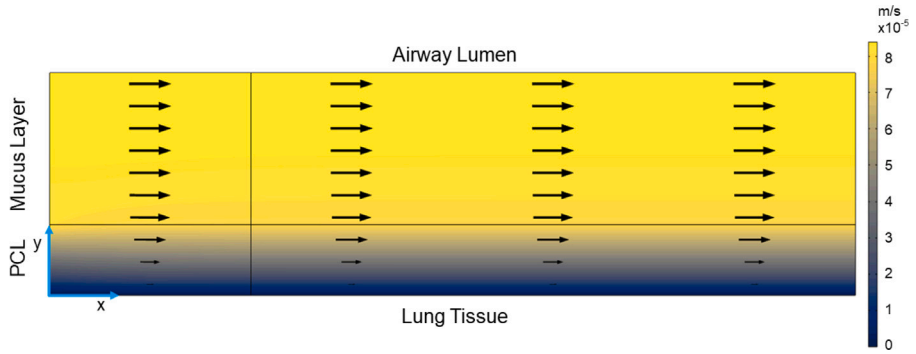

Fig. 4. Velocity profile for $L_m = 15$ μm. Arrows point in the direction of mucus flow and scale in size with the velocity. Note a nearly constant velocity throughout the mucus (upper) layer.

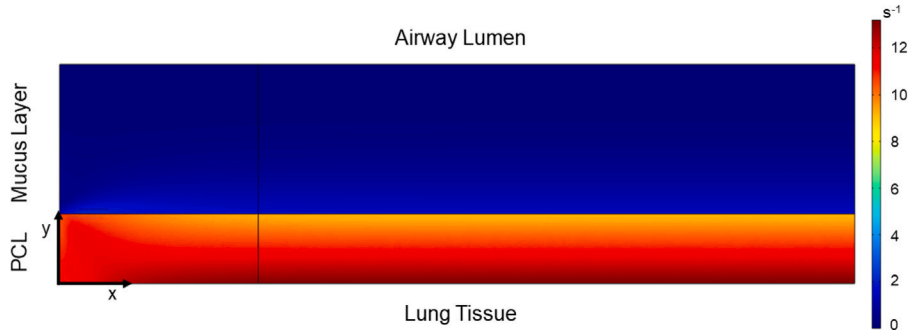

Fig. 5. Shear rate in the mucus (upper) and periciliary (lower) layers. The mucus (upper) layer has a comparatively small and constant shear rate due to its elasticity.

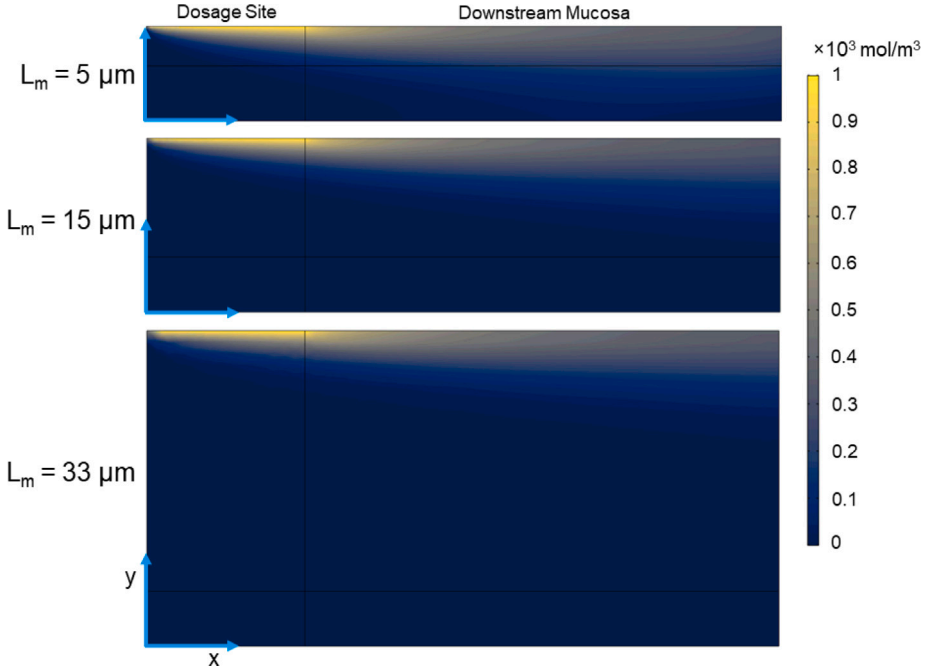

Fig. 6. Drug concentration profiles for particles with a radius $r_s = 20$ nm for various mucus thicknesses (from top to bottom): $L_m = 5$, 15, and 33 μm. The applied concentration constraint at the dosage site is 1000 $\mathrm{mol/m^3}$.

shown, highlighting the strong dependence of particle size on effective diffusivity. These sizes were chosen arbitrarily but are in the range of many viruses and engineered nanoparticles (Fig. 8). The profile for the $r_s = 20$ nm particle under these conditions is identical to the middle profile in Fig. 6. Larger particles are much more susceptible to steric hindrance in the mucus. While other factors are also at play, for many pathogens the basic reproduction number (R_0) seems to trend inversely with size, with large pathogens like tuberculosis being generally less infective than smaller pathogens like ebolavirus (Delamater et al., 2019) and SARS-CoV-2.

As expected, thicker mucus layers are more effective barriers to particle transport than thinner layers, and larger particles have lower diffusivities than those of smaller particles. This is generally true for passive diffusion in any fluid but is particularly relevant here as drug that

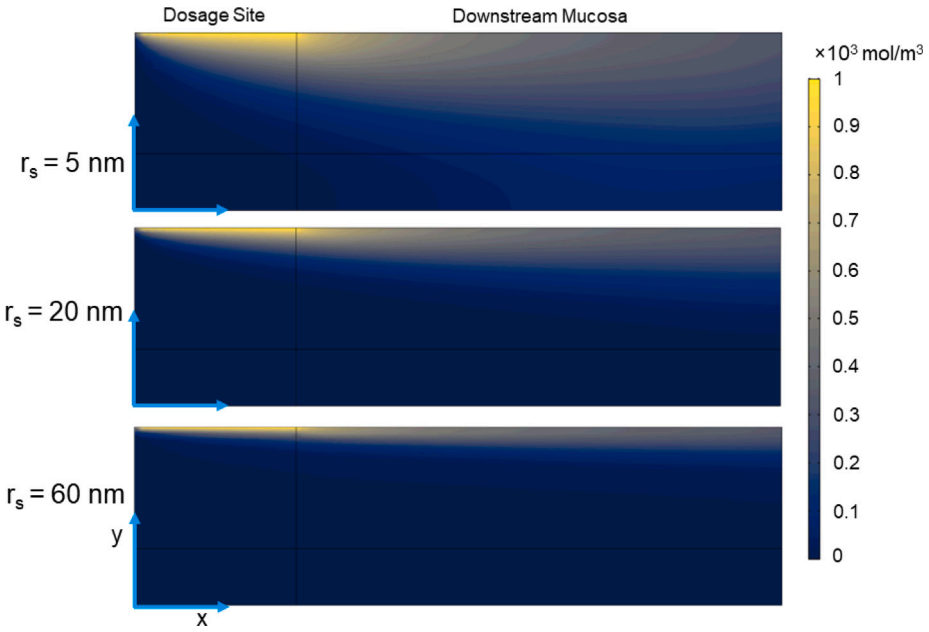

Fig. 7. Drug concentration profiles for a mucus thickness of $L_m = 15$ μm and particles with radii (from top to bottom): $r_s = 5$ nm, 20 nm, and 60 nm. The applied concentration constraint at the dosage site is 1000 mol/m^3.

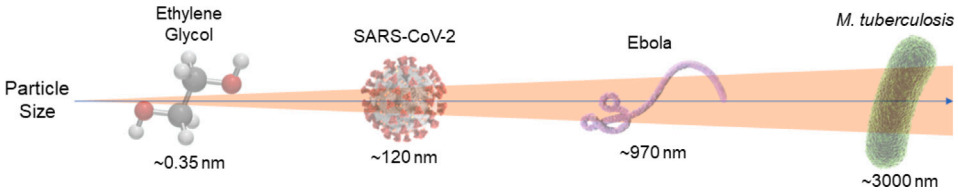

Fig. 8. Examples of molecules and pathogens on the size scale used in these simulations. Ethylene glycol was selected as a representative molecule because of the prevalence of using polymers consisting of ethylene glycol monomers for many drug delivery applications. Note: background wedge indicating size variations is not to scale.

does not fully cross both fluid layers is ultimately removed from the lungs by mucociliary clearance and then eliminated. Particles deposited deeper in the lungs will have greater success penetrating the mucus and reaching tissue (higher bioavailability) than the same particles deposited less deeply in the lungs.

Maximizing dose depth into airways is not always the goal, as certain patients may benefit from a specific localized dosage or tissue targeting along the conducting airways, such as in cancer treatment (Kolewe et al., 2021). For treatment regimes such as these, it is important to note that an appreciable amount of the applied drug only reaches the epithelium some distance upstream of the dosage site. For a particle in any mucus thickness, there is some distance upstream where the delivered dosage is maximized. By adding a cut line at the lung tissue epithelial surface and exporting the concentration results along this $y = 0$ line, this distance was found for various particle radius and mucus thickness combinations (Figs. 9 and 10). The smallest particles reach the epithelium quite close to the inlet (dosage site) when $L_m = 5$ μm, whereas in thicker mucus they reach the epithelium further from the inlet and have maxima that are smaller in magnitude than the thinnest mucus case. These results show how far a targeted "dosage site" for the applied drug needs to be upstream of the epithelial position where drug concentration is maximized. These results also could be integrated to determine the entire area under the curve, a common dosage metric for the total amount of the dosage that reaches the target location. We used 10^{-12} mol/m^3 as the minimum threshold concentration in Fig. 10 to ensure that the concentration that reaches the tissue is sufficiently large to be effective. Another important trend to notice is that increased particle size and mucus thickness both result in "flattening" of the curves shown in Figs. 9 and 10. Increases to either of these parameters result in the maxima occurring further downstream and being smaller in magnitude. When a treatment is designed, the simulation results for those drug particles can be used to calculate a dosage and delivery scheme. A dosage can be selected such that the desired uptake concentration to achieve a physiological response is achieved at the x-position corresponding to the maximum concentration (or a concentration above an acceptable threshold), and a dosage site selected based on the upstream distance required for this peak to occur at the target site. Alternatively, the area under the curve of the concentration that reaches the epithelium could be maximized for a given zone.

The model provides information regarding the magnitude of dosage delivered along the lung epithelium. However, factors that may optimize delivery such as shrinking the particle size or delivering deeper into the lungs may not be viable. Particle size causes variations in impaction with the mucus when inhaled (Schlosser et al., 2010), and a particle may require a protective coating to prevent side reactions, denaturation, or electrostatic entrapment (Huang et al., 2017; Halwes et al., 2018; Osman et al., 2018; Patil et al., 2018). It has been hypothesized that drugs may be applied to slow the beating of cilia, thereby decreasing mucus clearance and giving the drug more time to cross the fluid layers. This is an interesting idea, but many pathogenic diseases of the lung are directly caused by mucociliary clearance dysfunction, so this method would likely increase the risk of complications (Nawroth et al., 2019). In non-pathogenic diseases characterized by mucociliary clearance dysfunction such as cystic fibrosis, asthma, and COPD, steric (and electrostatic) hindrance is often highly accentuated due to higher-than-normal mucin concentrations. In these diseases, additional drugs (or even simply water) might be applied to cause the mucus to behave more like the healthy case and improve outcomes (Nafee et al., 2018).

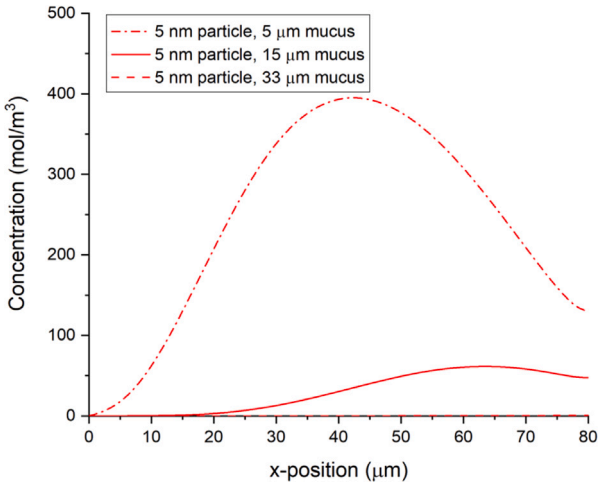

Fig. 9. Drug concentration at the epithelial surface $y = 0$ as a function of x-position in the steady-state model for particles with $r_s = 5\,\text{nm}$, where each curve has a different thickness of the mucus layer (L_m) indicated in the legend. The applied concentration constraint at the dosage site is 1000 mol/m^3.

One major limitation of the model is the assumption that electrostatic interactions are negligible. This assumption is valid for many particles including many viruses and polyethylene glycol-coated nanoparticles but certainly not all particles (Cahn et al., 2023). Mucins are anionic and lipophilic, so cationic or lipophilic particles are subject to electrostatic hindrance, which can be immobilizing (Hansing and Netz, 2018b). Repulsive anionic interactions between particles and mucins result in a sort of channel flow, which is less hindering but still causes an effective shrinkage of pores. Particles that are surface neutral but hydrophilic (either polar or zwitterionic) typically are the most successful at penetrating mucus in the absence of any form of active transport. Another limitation of the model is the assumption that a pulmonary surfactant layer plays no significant role in particle behavior. Although it is poorly understood, there exists a thin surface-active lipoprotein layer at the interface between the mucus and the airways. This surfactant layer is present even in the alveolar sacs and can bind to some species to negatively impact their ability to reach the epithelium (Kirch et al., 2012). While this layer likely has little impact on the movement of particles that also meet the electrostatic interaction limitation, many viruses and gene vectors are known to be destabilized or even trapped by interactions with the pulmonary surfactant (Kim et al., 2016). Particles that interact with this layer may suffer significant changes to their surface chemistry (generally becoming more lipophilic or cationic and more strongly attracted to surrounding surfactant molecules), but even among lipid-based gene vectors the effect of surfactant on behavior is variable and may be multimodal (Kim et al., 2016). As a result, it is likely a minor factor in the transport of all but the smallest vectors.

Unwanted side reactions may be an issue in many aerosolized drug applications, or side reactions could be desired in the case of a prodrug therapy. One specific application of interest is the simulation of prophylactics in the mucus. Lung mucosa, like other mucosal tissues, is an immunoactive region, with antibodies present in solution. Here, we considered a scenario when prophylactic antibodies against a virus particle have already been administered and are assumed to be uniformly distributed through the mucus in a zone. When these antibodies bind to an antigen (such as on the surface of a virus), the resulting complex is often trapped sterically or electrostatically. We simulated this reaction as an elementary irreversible reaction between two species:

$$A + B \rightarrow C \tag{9a}$$

$$R_C = k[A][B] = -R_A = -R_B \tag{9b}$$

where species A is the inhaled particle (simulating a virus), species B represents a prophylactic antibody present in the mucosa, and product C represents an antibody–antigen complex. For these simulations, the rate law coefficient was defined as $k = 0.05\,\text{m}^3/(\text{mol s})$. The applied concentration of A is $C_{A,i} = 1000\,\text{mol/m}^3$ at the dosage site (as in the other simulations), and the initial concentration of B is $C_{B,i} = 20\,\text{mol/m}^3$ present uniformly throughout the domain. Both concentrations were chosen arbitrarily; however, the radius of the viral particle A was set to $r_{s,A} = 60$ nm to simulate SARS-CoV-2 (Renu et al., 2020; Cascella et al., 2022). The radius of the particle B was set to $r_{s,B} = 6$ nm to simulate a monoclonal antibody (Hawe et al., 2011). We consider the complex C to be immobilized and thus has a diffusion coefficient of zero. The other two species have diffusion coefficients calculated using (3). Using these relationships, it can be shown whether a given level of antibody expression in the mucus is sufficient to prevent infection (defined as a certain amount of antigen reaching the epithelium) (Fig. 11). In these simulations, the diffusing particle is not a drug but a disease-causing viral particle. The model is equally capable of simulating the penetration of pathogens through the mucus as it is of therapeutic nanoparticles. Notice that some of species A persists at the rightmost boundary (Fig. 11) as all local concentration of B has been consumed. Species C has a notably different profile due to the immobilization of the species.

Using our model, users can solve for various unknowns when designing a drug delivery regimen. For example, for an existing drug particle of known size, a dosage site and dosage amount can be calculated via simulations such as those shown in Figs. 6 and 9. The efficacy of an administered prophylactic treatment may be screened via simulation of pathogenic exposure, such as that shown in Fig. 11, with the same approach being useful for simulation of prodrug therapies or controlled release of encapsulated drugs. The model can also predict whether a theoretical particle will significantly penetrate the mucus at all or be cleared from the body. The non-Newtonian physics of the mucus layer allows for the simulation of specific individual microenvironments or disease states by variation of only a few discrete variables that are simple to obtain experimentally. As many immunotherapies, especially those that are aerosolized, use spherical (or morphologically isotropic) particles, the model is well-suited to simulate these drugs, as relative diffusivities are calculated from the Stokes–Einstein equation. This means that morphologically anisotropic particles or pathogens, such as rod-shaped bacteria, spiral-shaped bacteria, and filamentous viruses will likely have behavior that deviates from the model. This is doubly true for pathogens that have evolved special mucopenetrative features, such as influenza type A (Vahey and Fletcher, 2019).

4. Conclusions

The model developed using COMSOL Multiphysics is a biologically realistic simulation of the mucociliary clearance mechanism. The model is customizable to the needs of the modeler or even the physiology of a patient, including both mucus properties and physical dimensions of the simulation domain. The administered particle is likewise customizable, although the model only accounts for steric and hydrodynamic hindrance. Existing simulations accounting for electrostatic interactions in "interacting gels" like mucus are computationally intense (Hansing and Netz, 2018a), and a macroscopic mathematical relationship that accounts for interactions may be added as an additional term to (3) as needed. By exporting transport simulation results, plots of concentration reaching the epithelium versus distance downstream from the dosage site were created. Using this information the optimal dosage site was identified for some test cases. Such information has relevance in the development of aerosolized drug treatments for localized diseased tissues, including tumors. One possible future refinement is replacing the concentration inlet with a time- and position-dependent step function, which simplifies the domain to only an upper mucus layer and lower PCL layer and adds possibilities for non-steady-state simulations.

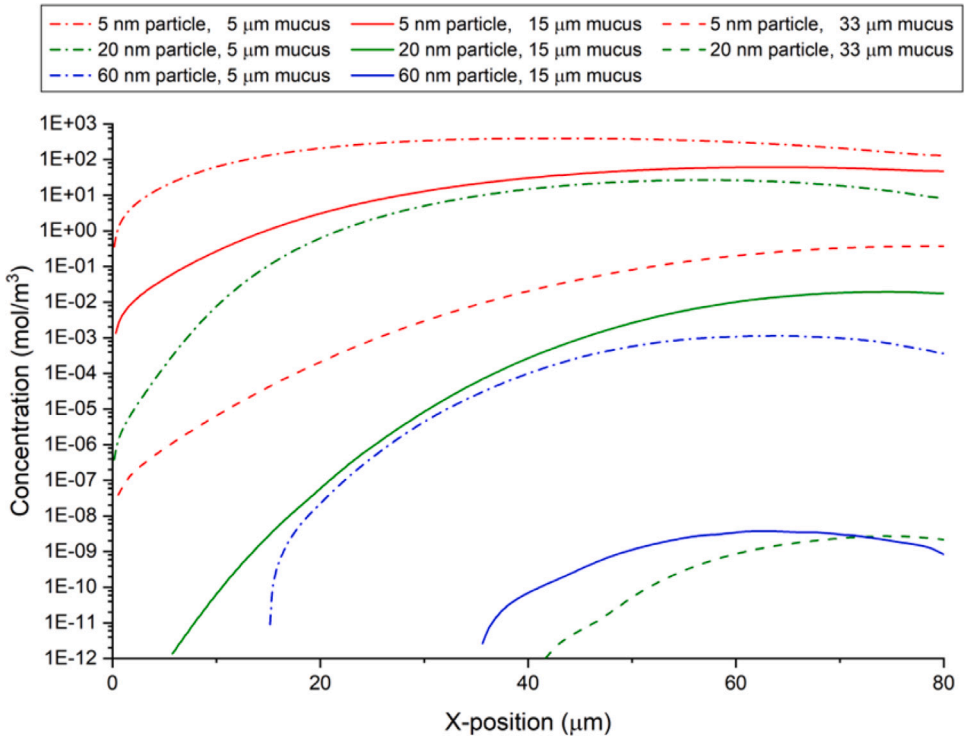

Fig. 10. Drug concentration (log scale) at the epithelial surface $y = 0$ as a function of x-position in the steady-state model for combinations of three mucus thicknesses (L_m) and particle sizes (r_s), selected for having values on similar orders of magnitude to demonstrate the interplay between particle size and mucus thickness. The applied concentration constraint at the dosage site is 1000 mol/m^3. Note that the case of $r_s = 60$ nm and $L_m = 33$ μm was also simulated, but the values are below the 10^{-12} mol/m^3 concentration threshold. The simulation tolerance was set to 10^{-12}. Consequently, concentrations below this tolerance should be considered negligible.

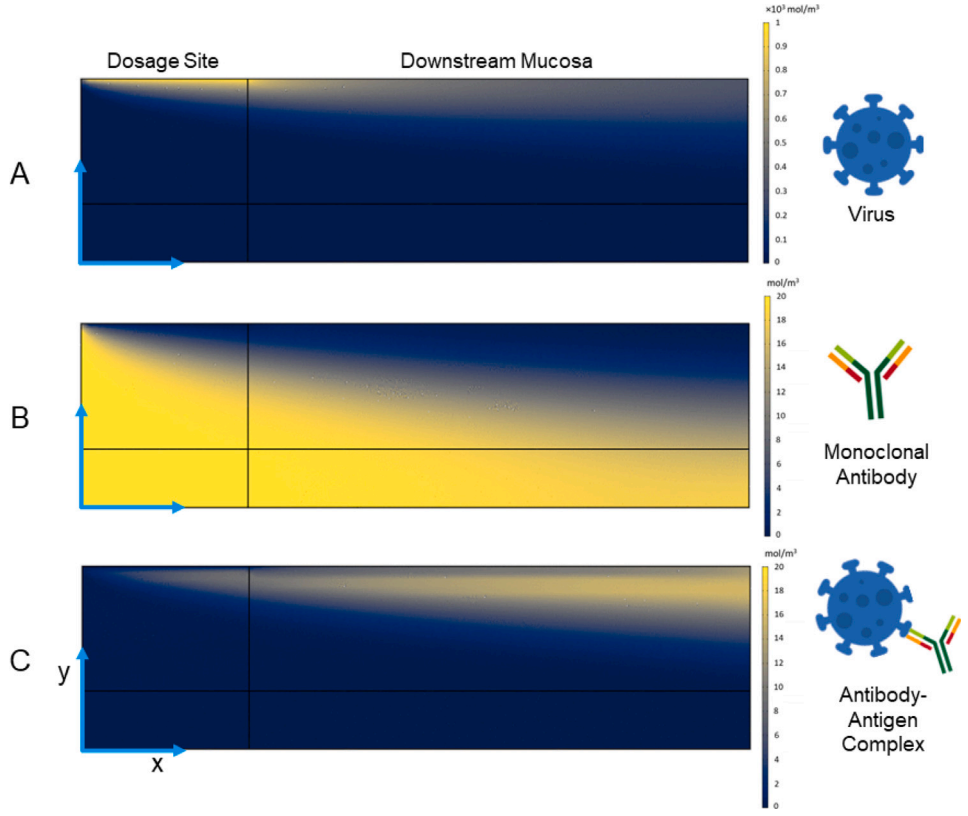

Fig. 11. Concentration profiles of the three interacting species, where species A (virus) is uniformly applied at the dosage site and species B (monoclonal antibody) is initially present uniformly throughout the domain. Species A and B are consumed by the reaction, and species C is the non-diffusing product (antibody–antigen complex).

CRediT authorship contribution statement

Blake A. Bartlett: Conceptualization, Methodology, Software, Formal analysis, Investigation, Writing – original draft. **Yu Feng:** Conceptualization, Methodology, Resources, Writing – review & editing. **Catherine A. Fromen:** Conceptualization, Resources, Writing – review & editing. **Ashlee N. Ford Versypt:** Conceptualization, Methodology, Supervision, Project administration, Writing – review & editing, Funding acquisition.

Declaration of competing interest

The authors declare that they have no known competing financial interests or personal relationships that could have appeared to influence the work reported in this paper.

Data availability

Data available at CFDparticleLungMucosa (Original data).

Acknowledgments

This work was supported by National Institutes of Health, United States grant R35GM133763 and Oklahoma State University, United States startup funds to Ashlee N. Ford Versypt. Blake A. Bartlett was supported by the Goldwater Scholar Program and the Freshman Research Scholar and Wentz Research Scholar Programs at Oklahoma State University, United States. We would like to thank Ford Versypt lab members and reviewers for their feedback on this manuscript.

References

Bartlett, B.A., Ford Versypt, A.N., 2023. CFDparticleLungMucosa. http://dx.doi.org/10.5281/zenodo.7901020, URL: https://github.com/ashleefv/CFDparticleLungMucosa. (Accessed 05 May 2023).

Button, B., Cai, L., Ehre, C., Kesimer, M., Hill, D.B., Sheehan, J.K., Boucher, R.C., Rubinstein, M., 2012. A periciliary brush promotes the lung health by separating the mucus layer from airway epithelia. Science 337, 937–941.

Cahn, D., Amosu, M., Maisel, K., Duncan, G.A., 2023. Biomaterials for intranasal and inhaled vaccine delivery. Nat. Rev. Bioeng. 1, 83–84.

Carlson, T.L., Lock, J.Y., Carrier, R.L., 2018. Engineering the mucus barrier. Annu. Rev. Biomed. Eng. 20, 197–220.

Cascella, M., Rajnik, M., Aleem, A., Dulebohn, S.C., Di Napoli, R., 2022. Features, Evaluation, and Treatment of Coronavirus (COVID-19). StatPearls Publishing.

Chateau, S., D'Ortana, U., Poncet, S., Favier, J., 2018. Transport and mixing induced by beating cilia in human airways. Front. Physiol. 9, 161.

Chen, Z., Zhong, M., Luo, Y., Deng, L., Hu, Z., Song, Y., 2019. Determination of rheology and surface tension of airway surface liquid: A review of clinical relevance and measurement techniques. Respir. Res. 20, 274.

Clarke, S.W., Pavia, D., 1980. Lung mucus production and mucociliary clearance: Methods of assessment. Br. J. Clin. Pharmacol. 9, 537–546.

Cone, R.A., 2005. Chapter 4: Mucus. In: Mestecky, J., Lamm, M.E., Ogra, P., Strober, W., Bienenstock, J., McGhee, J., Mayer, L. (Eds.), Mucosal Immunology, third ed. Academic Press, Cambridge, MA, pp. 49–72.

Cone, R.A., 2008. Barrier properties of mucus. Adv. Drug Deliv. Rev. 61, 75–85.

Cu, Y., Saltzman, M., 2009. Mathematical modeling of molecular diffusion through mucus. Adv. Drug Deliv. Rev. 61, 101–114.

Delamater, P.L., Street, E.J., Leslie, T.F., Yang, Y.T., Jacobsen, K.H., 2019. Complexity of the basic reproduction number (R_0). Emerg. Infect. Diseases 25, 1–4.

Duncan, G.A., Jung, J., Hanes, J., Suk, J.S., 2016. The mucus barrier to inhaled gene therapy. Mol. Ther. 24, 2043–2053.

Duncan, G.A., Kim, N., Colon-Cortes, Y., Rodriguez, J., Mazur, M., Birket, S.E., Rowe, S.M., West, N.E., Livraghi-Butrico, A., Boucher, R.C., Hanes, J., Aslanidi, G., Suk, J.S., 2018. An adeno-associated viral vector capable of penetrating the mucus barrier to inhaled gene therapy. Mol. Ther. Methods Clin. Dev. 9, 296–304.

Fahy, J.V., Dickey, B.F., 2010. Airway mucus function and dysfunction. N. Engl. J. Med. 363, 2233–2247.

Feng, Y., Chen, X., Yang, M., 2018. An *In Silico* investigation of a lobe-specific targeted pulmonary drug delivery method. In: Proc 2018 Design Med Devices Conf, Vol. 34. pp. 1–4.

Feng, Y., Chen, X., Yang, M., Dong, K., 2019. Multiscale computational models for respiratory aerosol dynamics with medical applications. Comput. Math. Methods Med. 2019, 1–2.

Halwes, M.E., Tyo, K.M., Steinbach-Rankins, J.M., Frieboes, H.B., 2018. Computational modeling of antiviral drug diffusion from poly(lactic-co-glycolic-acid) fibers and multicompartment pharmacokinetics for application to the female reproductive tract. Mol. Pharm. 15, 1534–1547.

Hansing, J., Netz, R.R., 2018a. Hydrodynamic effects on particle diffusion in polymeric hydrogels with steric and electrostatic particle-gel interactions. Macromolecules 51, 7608–7620.

Hansing, J., Netz, R.R., 2018b. Particle trapping mechanisms are different in spatially ordered and disordered interacting gels. Biophys. J. 114, 2653–2664.

Hastedt, J.E., Bäckman, P., Clark, A.R., Doub, W., Hickey, A., Hochhaus, G., Kuehl, P.J., Lehr, C., Mauser, P., McConville, J., Niven, R., Sakagimi, M., Weers, J.G., 2016. Scope and relevance of a pulmonary biopharmaceutical classification system AAPS/FDA/USP workshop March 16–17th, 2015 in Baltimore, MD. AAPS Open 2, 1–20.

Hawe, A., Hulse, W.L., Jiskoot, W., Forbes, R.T., 2011. Taylor dispersion analysis compared to dynamic light scattering for the size analysis of therapeutic peptides and proteins and their aggregates. Biophys. J. 28, 2302–2310.

Henning, A., Schneider, M., Nafee, N., Muijs, L., Rytting, E., Wang, X., Kissel, T., Grafahrend, D., Klee, D., Lehr, C., 2010. Influence of particle size and material properties on mucociliary clearance from the airways. J. Aerosol Med. Pulm. Drug Deliv. 23, 233–241.

Huang, X., Chrisholm, J., Zhuang, J., Xiao, Y., Duncan, G., Chen, X., Suk, J.S., Hanes, J., 2017. Protein nanocages that penetrate airway mucus and tumor tissue. Proc. Natl. Acad. Sci. USA 114, E6595–E6602.

Hussong, J., Lindken, R., Faulhammer, P., Noreikat, K., Sharp, K.V., Kummer, W., Westerweel, J., 2013. Cilia-driven particle and fluid transport over mucus-free mice tracheae. J. Biomech. 46, 593–598.

Islam, M.R., Feng, Y., 2023. Achieving targeted delivery of chemotherapeutic particles to small airway tumors via pulmonary route using endotracheal catheters: A CFPD study. Pharm 16, 158.

Johnson, E.M., Berk, D.A., Jain, R.K., Deen, W.M., 1996. Hindered diffusion in agarose gels: Test of effective medium model. Biophys. J. 70, 1017–1026.

Kim, N., Duncan, G.A., Hanes, J., Suk, J.S., 2016. Barriers to inhaled gene therapy of obstructive lung diseases: A review. J. Control. Release 240, 465–488.

King, M., Brock, G., Lundell, C., 1985. Clearance of mucus by simulated cough. J. Appl. Physiol. 58, 1776–1782.

Kirch, J., Guenther, M., Doshi, N., Schaefer, U.F., Schneider, M., Mitragotri, S., Lehr, C., 2012. Mucociliary clearance of micro- and nanoparticles is independent of size, shape, and charge–an ex vivo and in silico approach. J. Control. Release 159, 128–134.

Kleinstreur, C., Feng, Y., 2013. Computational analysis of non-spherical particle transport and deposition in shear flow with application to lung aerosol dynamics–a review. J. Biomech. Eng. 135, 021008.

Kolewe, E.L., Feng, Y., Fromen, C.A., 2021. Realizing lobe-specific aerosol targeting in a 3D-printed *in vitro* lung model. J. Aerosol Med. Pulm. Drug Deliv. 34, 42–56.

Korson, L., Drost-Hansen, W., Millero, F.J., 1969. Viscosity of water at various temperatures. J. Phys. Chem. 73, 34–39.

Lai, S.K., O'Hanlon, D.E., Harrold, S., Man, S.T., Wang, Y., Cone, R., Hanes, J., 2007. Rapid transport of large polymeric nanoparticles in fresh undiluted human mucus. Proc. Natl. Acad. Sci. USA 104, 1482–1487.

Lai, S.K., Wang, Y., Wirtz, D., Hanes, J., 2009. Micro- and macrorheology of mucus. Adv. Drug Deliv. Rev. 61, 86–100.

Lethem, M.I., 1993. The role of tracheobronchial mucus in drug administration to the airways. Adv. Drug Deliv. Rev. 11, 271–298.

Matsui, H., Randell, S.H., Peretti, S.W., Davis, C.W., Boucher, R.C., 1998. Coordinated clearance of periciliary liquid and mucus from airway surfaces. J. Clin. Invest. 102, 1125–1131.

Meziu, E., Koch, M., Fleddermann, J., Schwarzkopf, K., Schneider, M., Kraegeloh, A., 2021. Visualization of the structure of native human pulmonary mucus. Int. J. Pharm. 597, 1–9.

Murgia, X., Loretz, B., Hartwig, O., Hittinger, M., Lehr, C., 2018. The role of mucus on drug transport and its potential to affect therapeutic outcomes. Adv. Drug Deliv. Rev. 124, 82–97.

Nafee, N., Forier, K., Braeckmans, K., Schneider, M., 2018. Mucus-penetrating solid lipid nanoparticles for the treatment of cystic fibrosis: Proof of concept, challenges and pitfalls. Eur. J. Pharmaceut. Biopharmaceut. 124, 125–137.

Nawroth, J.C., van der Does, A.M., Ryan (Firth), A., Kanso, E., 2019. Multiscale mechanics of mucociliary clearance in the lung. Phil. Trans. R. Soc. 375, 1–8.

Norton, M.M., Robinson, R.J., Weinstein, S.J., 2011. Model of mucociliary clearance and the role of mucus rheology. Phys. Rev. E 83, 011921.

Osman, G., Rodriguez, J., Chan, S.Y., Chisholm, J., Duncan, G., Kim, N., Tatler, A.L., Shakesheff, K.M., Hanes, J., Suk, J.S., Dixon, J.E., 2018. PEGylated enhanced cell penetrating peptide nanoparticles for lung gene therapy. J. Control. Release 285, 35–45.

Patil, H.P., Freches, D., Karmani, L., Duncan, G.A., Ucakar, B., Suk, J.S., Hanes, J., Gallez, B., Vanbever, R., 2018. Fate of PEGylated antibody fragments following delivery to the lungs: Influence of delivery site, PEG size and lung inflammation. J. Control. Release 272, 62–71.

Philips, R.J., 2000. A hydrodynamic model for hindered diffusion of proteins and micelles in hydrogels. Biophys. J. 79, 3350–3354.

Renu, K., Prasanna, P.L., Abilash, V.G., 2020. Coronaviruses pathogenesis, comorbidities and multi-organ damage–a review. Life Sci. 255, 117839.

Rohatgi, A., 2022. Webplotdigitizer: Version 4.6. URL: https://automeris.io/WebPlotDigitizer.

Ruge, C.A., Kirch, J., Lehr, C., 2013. Pulmonary drug delivery: From generating aerosols to overcoming biological barriers–therapeutic possibilities and technological challenges. Lancet Respir. Med. 1, 402–413.

Schlosser, P.M., Asgharian, B.A., Medinsky, M., 2010. Inhalation exposure and absorption of toxicants. In: McQueen, C.A. (Ed.), Comprehensive Toxicology, second ed. Elsevier Science, New York, NY, pp. 75–109.

Schuster, B.S., Suk, J.S., Woodworth, G.F., Hanes, J., 2013. Nanoparticle diffusion in respiratory mucus from humans without lung disease. Biomaterials 34, 3439–3446.

Shahsavari, S., McKinley, G.H., 2015. Mobility of power-law and carreau fluids through fibrous media. Phys. Rev. E 92, 063012.

Shete, H.K., Vyas, S.S., Patravale, V.B., Disouza, J.I., 2014. Pulmonary multifunctional nano-oncological modules for lung cancer treatment and prevention. J. Biomed. Nanotechnol. 10, 1863–1893.

Sims, L.B., Miller, H.A., Halwes, M.E., Steinbach-Rankins, J.M., Frieboes, H.B., 2019. Modeling of nanoparticle transport through the female reproductive tract for the treatment of infectious diseases. Eur. J. Pharmaceut. Biopharmaceut. 138, 37–47.

Smith, D.J., Gaffney, E.A., Blake, J.R., 2008. Modelling mucociliary clearance. Respir. Physiol. Neurobiol. 163, 178–188.

Taherali, F., Varum, F., Basit, A.W., 2018. A slippery slope: On the origin, role and physiology of mucus. Adv. Drug Deliv. Rev. 124, 16–33.

Tang, B.C., Dawson, M., Lai, S.K., Wang, Y., Suk, J.S., Yang, M., Zeitlin, P., Boyle, M.P., Fu, J., Hanes, J., 2009. Biodegradable polymer nanoparticles that rapidly penetrate the human mucus barrier. Proc. Natl. Acad. Sci. USA 106, 19268–19273.

Vahey, M.D., Fletcher, D.A., 2019. Influenza a virus surface proteins are organized to help penetrate host mucus. eLife 8, e43764.

Vélez-Cordero, J.R., Lauga, E., 2013. Waving transport and propulsion in a generalized Newtonian fluid. J. Non-Newton. Fluid Mech. 199, 37–50.

Wolff, R.K., 1986. Effects of airborne pollutants on mucociliary clearance. Environ. Health Perspect. 66, 223–237.

World Health Organization, 2020. Global health estimates 2020: Deaths by cause, age, sex, by country and by region, 2000–2019. URL: https://www.who.int/data/gho/data/themes/mortality-and-global-health-estimates/ghe-leading-causes-of-death.

Yeates, D.B., Aspin, N., Levison, H., Jones, M.T., Bryan, A.C., 1975. Mucociliary tracheal transport rates in man. J. Appl. Physiol. 39, 487–495.